Biomaterials 31 (2010) 2163–2175

Contents lists available at ScienceDirect

Biomaterials

journal homepage: www.elsevier.com/locate/biomaterials

The regulation of tendon stem cell differentiation by the alignment of nanofibers

Zi Yin [a,b,1], Xiao Chen [a,b,1], Jia Lin Chen [a,b], Wei Liang Shen [a,c], Thi Minh Hieu Nguyen [d], Ling Gao [f], Hong Wei Ouyang [a,b,e,*]

[a] Center for Stem Cell and Tissue Engineering, School of Medicine, Zhejiang University, China
[b] Department of Sports Medicine, School of Medicine, Zhejiang University, China
[c] Department of Orthopedic Surgery, 2nd Affiliated Hospital, School of Medicine, Zhejiang University, China
[d] Division of Bioengineering, National University of Singapore, Singapore
[e] Institute of Cell Biology, School of Medicine, Zhejiang University, China
[f] School of Medicine, Zhejiang University, China

ARTICLE INFO

Article history:
Received 24 October 2009
Accepted 24 November 2009
Available online 7 December 2009

Keywords:
Tendon stem cells
Aligned nanofiber
Differentiation
Tendon regeneration
Mechanotransduction

ABSTRACT

Tendon is a specific connective tissue composed of parallel collagen fibers. The effect of this tissue-specific matrix orientation on stem cell differentiation has not been investigated. This study aimed to determine the effects of nanotopography on the differentiation of human tendon stem/progenitor cells (hTSPCs) and develop a biomimetic scaffold for tendon tissue engineering. The immuno-phenotype of fetal hTSPCs was identified by flow cytometry. The multipotency of hTSPCs toward osteogenesis, adipogenesis, and chondrogenesis was confirmed. Then, the hTSPCs were seeded onto aligned or randomly-oriented poly (L-lactic acid) nanofibers. Scanning electron micrographs showed that hTSPCs were spindle-shaped and well orientated on the aligned nanofibers. The expression of tendon-specific genes was significantly higher in hTSPCs growing on aligned nanofibers than those on randomly-oriented nanofibers in both normal and osteogenic media. In addition, alkaline phosphatase activity and alizarin red staining showed that the randomly-oriented fibrous scaffold induced osteogenesis, while the aligned scaffold hindered the process. Moreover, aligned cells expressed significantly higher levels of integrin α1, α5 and β1 subunits, and myosin II B. In *in vivo* experiments, the aligned nanofibers induced the formation of spindle-shaped cells and tendon-like tissue. In conclusion, the aligned electrospun nanofiber structure provides an instructive microenvironment for hTSPC differentiation and may lead to the development of desirable engineered tendons.

1. Introduction

Tendon injuries, which happen frequently during sports and other rigorous activities, are a common clinical problem due to the poor regeneration ability of tendons [1]. The traditional treatments for repair or replacement of damaged tendons, including autografts, allografts, xenografts, and prosthetic devices, rarely have satisfactory results and have some inevitable disadvantages such as donor site morbidity, risk of disease transmission, and limited long-term function [2–5]. Therefore, tendon tissue engineering has been receiving increasing attention as a potential strategy to treat tendon injuries.

Two of the most essential elements of tendon tissue engineering are seed cells and the scaffold. The seed cells widely used in tendon tissue engineering are mesenchymal stem cells and fibroblasts [6–9]. However, how to induce mesenchymal stem cells to differentiate into tendon-forming cells and avoid ossification *in vivo* still remains a great challenge, and this hinders their application [10]. On the other hand, the limited capacity of fibroblasts to proliferate inevitably influences the final outcome of regeneration [11]. Only recently has success been achieved in identifying human tendon stem/progenitor cells (hTSPCs), which are derived from human tendon. They exhibit universal stem cell characteristics such as clonogenicity, self-renewal, and multipotent differentiation capacity [12]. Human TSPCs (passage 2) are positive for CD146 (also known as Muc18 or MCAM), CD90 and CD44, but not for CD18 (a surface receptor on bone marrow stromal cells) and CD34 (the hematopoietic cell marker) [12]. Also, the multidifferentiation potential of hTSPCs toward osteogenesis, adipogenesis, and chondrogenesis has been determined [12]. The great potential of hTSPCs for tendon differentiation opens new possibilities for tendon regeneration [12]. However, an ideal substrate for hTSPC differentiation remains to be discovered.

* Corresponding author. Mailbox 39, Center for Stem Cell and Tissue Engineering, School of Medicine, Zhejiang University, 388 Yu Hang Tang Road, Hangzhou 310058, China. Tel./fax: +86 571 88208262.
E-mail address: Hwoy@zju.edu.cn (H.W. Ouyang).
[1] These authors contributed equally in this study.

0142-9612/$ – see front matter © 2009 Elsevier Ltd. All rights reserved.
doi:10.1016/j.biomaterials.2009.11.083

The topography of the extracellular microenvironment plays an important role in cellular activity, from attachment and morphology to proliferation and differentiation though contact guidance [13–18]. Both the matrix-elasticity and the substrate patterning influence the specification of stem cell lineage [19,20]. It is known that hTSPCs reside within a niche that comprises primarily parallel collagen fibers, and this niche plays an important role in regulating their function and differentiation [12,21,22]. As electrospinning is a straightforward, cost-effective method to replicate natural extracellular matrix, we fabricated a biomimetic aligned poly (L-lactic acid) (PLLA) fibrous scaffold, and hypothesized that the aligned electrospun nanofibers regulate hTSPC orientation and differentiation.

Cells sense matrix topography and transduce this information into morphological changes. A cellular mechano-transducer is required to pull against the matrix and thereby affect the direction of differentiation [19]. It has been suggested that extracellular matrix and integrin collaborate to modulate both cell shape and the intracellular signal [23]. However, the mechanism by which nanotopographical cues instruct cell orientation and morphology, and further enhance cell differentiation to a specific lineage, is still poorly understood.

The present study aimed to investigate whether aligned nanofibers influence hTSPC differentiation, as well as the mechanism involved. The activity of hTSPCs on aligned nanofibers was investigated and compared with randomly-oriented nanofibers. Also, the efficacy of aligned nanofibers in inducing tendon tissue regeneration was investigated *in vivo*.

2. Materials and methods

2.1. Fabrication of PLLA scaffold

Electrospinning is widely used to fabricate nanofibrous scaffolds with required sizes and dimensions by manipulating system and process parameters [24]. Therefore, we employed this controllable, reproducible, and relatively simple method to fabricate the nanofibrous scaffolds. PLLA was chosen as the biomaterial due to its good biocompatibility and biodegradability. In order to investigate the effects of structural alignment on hTSPC differentiation, randomly-oriented fibrous membranes with similar fiber diameters served as controls. Both aligned and randomly-oriented PLLA scaffolds were fabricated using the electrospinning technique under optimum conditions. The polymer solution was prepared by dissolving PLLA (Ji'nan Daigang Biomaterial Co., Ltd) into chloroform/ethanol (3:1) at the concentration of 3% (aligned) or 2% (random) for more than 2 days to allow complete dissolution and to achieve comparable diameters. The solution was then fed into a 12-ml plastic syringe, which was controlled by a syringe pump with a rate of 2 ml/h. A high voltage (12 kV) was applied to the needle tip, which was placed 10 cm above the collector. A flat aluminum plate was used to collect the random fibers. The collector for aligned fibers was a disk rotating at 4000 rpm. The resulting scaffolds were then transferred to cover slips and sterilized with ethanol and UV overnight before they were used for cell culture. Nanofibers were collected for 2–3 h, resulting in a fiber mat ranging in thickness from 0.14 to 0.17 mm. The aligned and randomly-oriented scaffolds used in this study were of similar thickness and distribution.

2.2. Structural morphology of PLLA scaffold

The scaffold samples were sputter-coated with gold, and then their structure was observed under scanning electron microscopy (SEM) (Hitachi S3000N) at an accelerating voltage of 15 kV. After the micrographs were obtained, image analysis software (UTHSCSA ImageTool 3.0) was used to measure the average diameter and angle distribution (with respect to the vertical axis) of the nanofibers ($n = 3$). For each sample, an average of 60 nanofibers was counted.

2.3. Biomechanical test

Mechanical testing was performed using an Instron tension/compression system with a 10 N load cell (Instron, Canton, MA) with precision of 0.001 N, and Fast-Track software (Model 5543, Instron, Canton, MA). Extensor tendons isolated from a New England rabbit (3 kg) were used as comparison. Aligned and randomly-oriented nanofiber-based sheet specimens were prepared ($n = 5$ for each group). The size of each specimen was $10 \times 50 \times 0.15$ mm. The sample was fixed to custom-made clamps. The load was applied along the direction of fibers on the aligned scaffolds. After applying a preload of 0.02 N, each scaffold underwent a load to failure test at an elongation rate of 5 mm/min. The load–elongation behavior of the scaffolds and failure modes were recorded. The structural properties of the scaffolds were represented by stiffness (N/mm), failure force (N), and modulus (MPa). For each scaffold, the greatest slope in the linear region of the load–elongation curve over a 1% elongation interval was used to calculate stiffness. Construct modulus was determined from these data based on the sample geometry and measured gauge length.

2.4. Cell isolation and culture

We obtained human fetal Achilles tendon samples from an aborted embryo (age 5 months) following the approved guidelines set by the Women's Hospital School of Medicine Zhejiang University Institutional Review Board and Institutional Animal Care and Use Committee. We cut the tendon tissue into 1–2 mm^3 pieces, and washed them three times with phosphate-buffered saline (PBS). The tissue fragments were digested with 0.25% collagenase (Sigma) overnight at 37 °C. Single cell suspensions were cultured in Dulbecco's modified Eagle's medium (DMEM, low glucose; Gibco, Grand Island, NY, http://www.invitrogen.com) with 10% fetal bovine serum (FBS; Invitrogen, Carlsbad, CA, http://www.invitrogen.com-Gibco) and 1% penicillin–streptomycin (Gibco). The medium was changed every 3 days.

2.5. Monocloning selection

The cells were cultured in DMEM supplemented with penicillin–streptomycin and 20% FBS. Most of the cells in culture appeared fibroblast-like after two passages and were then seeded at very low density (2 cells/cm^2) to form colonies. After 10–12 days, the colonies formed were stained with 1% crystal violet (Sigma, St. Louis, MO, http://www.sigmaaldrich.com) in methanol for 10 min. The number and size of all colonies with diameters >2 mm were counted. The human tendon-derived colonies forming fibroblast-like cells were designated as hTSPCs. All hTSPCs in this study were of polyclonal origin. The cells were trypsinized when confluent and split 1:5. Cells were used between passages 4 and 6.

2.6. Fluorescence-activated cell sorting (FACS) analysis

Cells (5×10^5) were incubated with 1 μg of PE- or FITC-conjugated mouse specific to human monoclonal antibodies for 1 h at 4 °C. PE- or FITC-conjugated isotype-matched IgGs (BD Pharmingen) were used as controls. All antibody conjugates were from Pharmingen/BD Biosciences unless specified otherwise. They were FITC-conjugated mouse specific antibodies to human CD18 (clone 6.7, IgG1, κ), CD34 (581, IgG1, κ), CD90 (5E10, IgG1, κ), and PE-conjugated mouse specific antibody to human CD44 (515, IgG1, κ). The non-conjugated mouse specific antibody to human CD105 was incubated with 1×10^6 cells for 1 h at 4 °C. After washing, the cells were incubated with FITC-conjugated rabbit anti-mouse IgG for 45 min on ice. After washing, the samples were analyzed using a Coulter Epics XL flow cytometer.

2.7. Multipotent differentiation

We studied the *in vitro* multidifferentiation potential of the hTSPCs toward osteogenesis, adipogenesis, and chondrogenesis as described previously [6,12,25]. Osteogenic induction: hTSPCs were plated at low density (10^3 cells/cm^2) on tissue-culture-treated dishes in the presence of 10 mM b-glycerol phosphate (Sigma), 0.1 μM dexamethasone (Sigma), and 50 μg/ml ascorbic acid (Sigma) in DMEM-high glucose containing 10% FBS and 1% penicillin–streptomycin for 4 weeks. The media were changed every 3 days. Data were confirmed in 4 independent experiments. Adipogenic induction: hTSPCs were grown to confluence followed by exposure to 1 mM dexamethasone, 10 μg/ml insulin, and 0.5 mM isobutylxanthine (all from Sigma) in DMEM-high glucose containing 10% FBS and 1% penicillin–streptomycin for 3 weeks. The media were changed every 3 days. Data were confirmed in 4 independent experiments. Chondrogenic induction: Differentiation of hTSPCs was induced in pellet culture by exposure to 10 ng/ml TGF-β3 (Millipore) and 200 μM ascorbic acid (Sigma) in DMEM-high glucose medium for 4 weeks. Adherent cell colonies were trypsinized and counted. Aliquots of 2×10^5 cells in 0.5 ml of medium were then centrifuged at 500*g* in 15 ml polypropylene conical tubes. Within 24 h after incubation, the cells formed an aggregate that did not adhere to the walls of the tube. The medium was changed every two or three days, and cell aggregates were obtained at intervals of as long as 21 days. Data were confirmed in 3 out of 4 independent experiments.

2.8. SEM observation

hTSPCs were seeded onto PLLA scaffolds at 2×10^4 cells/cm^2. Two days after seeding, the cell morphology and distribution were visualized using SEM. Specimens were fixed in 0.25% glutaraldehyde solution, then rinsed 3 times in PBS, 30 min each time. The specimens were immersed in OsO_4 for 40 min and then rinsed 3 times in PBS, 30 min each time, and dehydrated in increasing concentrations of acetone (30–100% v/v). After drying, the specimens were mounted on aluminum stubs and coated with gold, then viewed in a Hitachi S-3000N SEM at an accelerating voltage of 15 kV.

2.9. Cell labeling and detection

The CFDA molecular probe is well recognized as a marker of viable cells. To investigate whether the nuclei also had aligned morphology like tenocytes *in vitro*, we stained the cytoplasm with CFDA and the nuclei with propidium iodide (Sigma). The day after seeding cells on the scaffolds, the cell-scaffold constructs were incubated with 25 μg/ml CFDA SE (Molecular Probes Inc.) for 15 min, and then washed with PBS. Live cells were observed under a laser confocal microscope (Zeiss LSM-510). Then, cell-scaffold constructs were fixed in 4% paraformaldehyde for 15 min and incubated with 100 μg/ml propidium iodide (Sigma) for 10 min.

2.10. Cell proliferation assay

Cell viability and proliferation were measured with a Cell Counting KIT-8 (CCK-8, Dojindo, www.dojindo.cn). The hTSPC-seeded aligned and randomly-oriented scaffolds, at desired time points, were incubated in CCK-8 solution in a 5% CO_2 incubator at 37 °C for 3 h. The intense orange-colored formazan derivative formed by cell metabolism is soluble in the culture medium. The absorbance was measured at 450 nm with a reference wavelength of 650 nm. Cell number was correlated to optical density (OD).

2.11. Alkaline phosphatase (ALP) and alizarin red staining for mineralization

hTSPCs (10^4/cm^2) were seeded onto scaffolds and cultured in osteogenic induction medium. After 2 weeks, ALP activity was assayed using a BCIP/NBT alkaline phosphatase color development kit (Beyotime Institute of Biotechnology). DAPI (Beyotime Institute of Biotechnology) was used to stain nuclei. ALP-positive cells were counted under a light microscope (Olympus IX71) in five randomly-selected fields. Calcium deposits were detected by staining with 2% alizarin red S (pH 4.2; Sigma). To quantify the stained nodules, the stain was solubilized with 0.5 ml 5% SDS in 0.5 N HCl for 30 min at room temperature. Solubilized stain (0.15 ml) was transferred to wells of a 96-well plate, and absorbance was measured at 405 nm [26]. Data are presented as mean ± SD, $n = 3$.

2.12. Real-time PCR

To evaluate the effect of aligned nanotopography on tendon-lineage differentiation, the expression of tendon-specific markers at the mRNA level was examined in hTSPCs cultured on the scaffolds in normal media for 3 or 7 days. To explore how the cells sense and respond to the matrix topography, expression of α1, α5, and β1 integrin subunits were assessed using real-time PCR. Total cellular RNA was isolated by lysis in TRIzol (Invitrogen). The levels of tendon-specific genes and transcription factors in hTSPCs cultured on aligned and random fibrous scaffolds were assessed by quantitative PCR. hTSPCs from just before seeding served as control. PCR was performed using a Brilliant SYBR Green QPCR Master Mix (TakaRa) on a Light Cycler apparatus (ABI 7900HT). The PCR cycling consisted of 40 cycles of amplification of the template DNA with primer annealing at 60 °C. The relative level of expression of each target gene was then calculated using the $2^{-\Delta\Delta Ct}$ method [27]. The amplification efficiencies of primer pairs were validated to enable quantitative comparison of gene expression. All primers (Invitrogen) were designed using primer 5.0 and are summarized in Table 1. Each real-time PCR was performed on at least 5 different experimental samples; representative results are shown as target gene expression normalized to β-actin. Error bars reflect one standard deviation from the mean of technical replicates as described in [28].

2.13. Cell labeling and detection

To genetically identify hTSPCs within the site of implantation *in vivo*, the cells were stained with DiI, which is stable in paraffin sections [3]. Briefly, when the cells had reached 80% confluency, the DiI was diluted in the culture medium to achieve a final concentration of 10 μg/mL. Cells were suspended (10^6/ml) and incubated for 30 min at 37 °C, then washed twice in PBS. The DiI fluorescence was measured with a fluorescence microscope (BX41; Olympus, Japan) at an excitation wavelength of 543 nm.

2.14. Animal model

The University of Zhejiang Institutional Animal Care and Use Committee approved the study protocol (permit No. zju2008101002). To test the cytotoxicity of the scaffolds, we did intramuscular implantations on 8–10-week-old female mice ($n = 6$). A lateral incision was made on the hind limb. Scaffolds were cut into 5 × 5 × 0.15 mm pieces ($n = 6$) and buried in the gastrocnemius. Then the incision was closed with 3–0 non-absorbable silk suture. Animals were sacrificed by anesthetic overdose, 1 or 6 weeks after implantation. In order to determine the induction potential of the aligned scaffold in the *in vivo* environment, cells with scaffolds were implanted into a nude mouse model. This model is superior to monolayer culture in that it provides a more natural environment and affords the ability to perform 3D histologic evaluation of the implants. After hTSPCs had been growing on scaffold for 3 days, we transplanted the constructs subcutaneously into immunocompromised mice. After anesthesia, an incision was made on the dorsum and a subcutaneous pocket of 2 cm was created. We implanted scaffolds (2× 4 cm, 2–2.5 × 10^4 cells/cm^2, $n = 3$) subcutaneously into the dorsal surface of 8–10-week-old female immunocompromised athymic nude mice (Harlan, $n = 3$) [12]. We harvested the transplants 1 week later.

Table 1
Primer sequences used for reverse transcription-polymerase chain reaction gene expression analysis.

Genes	5′–3′	Primers	Production size (bp)
Beta-actin	Forward	AGCGAGCATCCCCCAAAGTT	285
	Reverse	GGGCACGAAGGCTCATCATT	
Collagen I	Forward	ATGGATTCCAGTTCGAGTAGGC	246
	Reverse	CATCGACAGTGACGCTGTAGG	
Collagen III	Forward	TTTTGCAGTGATATGTGATGTT	125
	Reverse	GGATGGTGGTTTTCAGTTTA	
Collagen XIV	Forward	AAGGATTGCCCTCCGACTAC	319
	Reverse	GATGCGTTCATTGCCTTCTC	
Scleraxis	Forward	CGAGAACACCCAGCCCAAAC	143
	Reverse	ACCTCCCCCAGCAGCGTCT	
Eya 2	Forward	CGTTGGTGGGTTGATAGG	174
	Reverse	AGGGCAGGAATTAGTTGAGT	
Elastin	Forward	GCAGTGCCTGGGGTCCTTGGAG	211
	Reverse	GCTGCTTTAGCGGCTGCAGCTGG	
Runx2	Forward	GTGATAAATTCAGAAGGGAGG	118
	Reverse	CTTTTGCTAATGCTTCGTGT	
Alkaline phosphatase	Forward	ATGTCTGGAACCGCACTGAA	237
	Reverse	CGCCTGGTAGTTGTTGTGAGCATAG	
Osteocalcin	Forward	AGGGCAGCGAGGTAGTGAAGA	181
	Reverse	TAGACCGGGCCGTAGAAGC	
Integrin α1	Forward	AAGGGGAGAACTTCGGAGTGA	167
	Reverse	AAATGAGCAGCATTAACAGCAAC	
Integrin α5	Forward	CCAATCACCCCATTAACCCAAA	113
	Reverse	GATCTGAGGTCCCGAGGAAGCA	
Integrin β1	Forward	TTCAGTGAATGGGAACAACGA	125
	Reverse	ATGCAAGGCCAATAAGAACAA	
Myosin II B	Forward	GCCGCCAACAAATTAGTCCGT	138
	Reverse	GCGTTTAAGCTGCTTCATCCGA	

2.15. Histological examination and Masson trichrome staining

Specimens were immediately fixed in 10% neutral buffered formalin, dehydrated through an alcohol gradient, cleared, and embedded in paraffin blocks. Histological sections (10 μm) were prepared using a microtome and subsequently stained with hematoxylin and eosin. In addition, Masson trichrome staining was done according to standard procedures to examine the general appearance of the collagen fibers.

2.16. Determination of collagen content

The amount of deposited collagen in the scaffold was quantified using a collagen assay kit and following the manufacturer's protocol (Jiancheng Ltd., Nanjing, China).

2.17. Statistical analysis

Statistical analysis of data for gene expression was carried out by analysis of variance (ANOVA) to determine the presence of any significant difference between groups, followed by LSD (least significant difference) test to determine the values that were significantly different. Differences were considered statistically significant at $^{*}p < 0.05$. Student's *t*-test was used to evaluate the statistical significance of mechanical properties. Significance level was set at $^{***}p < 0.001$.

3. Results

3.1. Identification and characterization of hTSPCs

The human fetal tendon-derived cells showed fibroblast-like morphology (Fig. 1 A). To determine whether the cells were clonogenic, we generated and cultured single cell suspensions. A portion of tendon-derived cells attached to the plate and remained quiescent for 3–5 days before they started rapidly dividing to form colonies. After 10–12 days, colonies that had formed from single cells were visualized using methyl violet staining (Fig. 1B and C). Five to six percent of tendon-derived cells at passage 2 were able to form colonies.

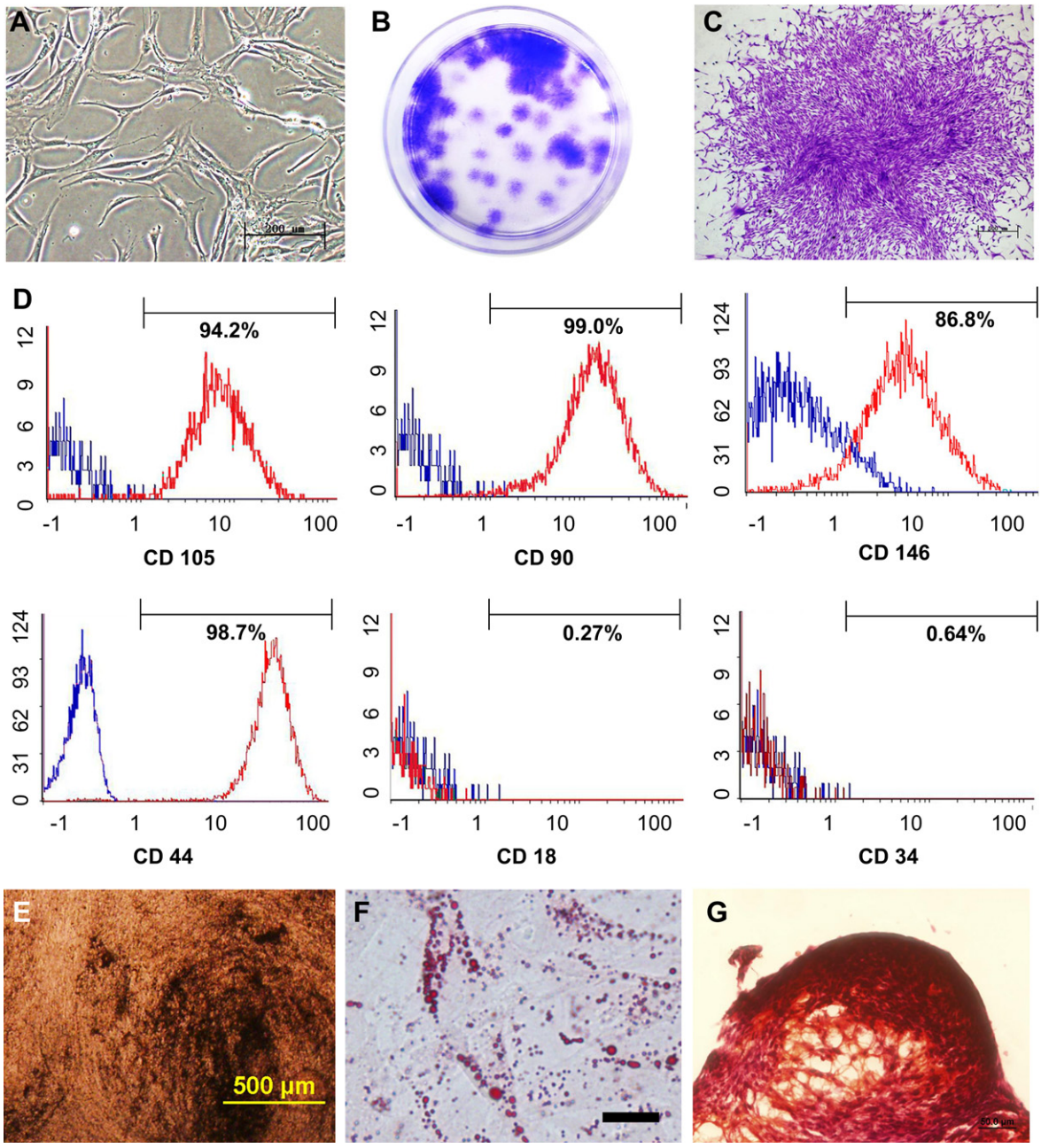

Fig. 1. Isolation and characterization of human tendon stem cells. (A) Morphology of human tendon-derived cells at P2. (B) Methyl violet staining to visualize colonies formed by hTSPCs. (C) Morphology of a formed colony. (D) Flow cytometry analysis of the expression of indicated cell surface markers related to mesenchymal stem cells and hematopoietic stem cells in hTSPCs. (E) Von Kossa staining showing osteogenic differentiation of hTSPCs. (F) Oil red O staining showing adipogenic differentiation of hTSPCs. (G) Chondrogenic differentiation of hTSPCs revealed by safranin O staining. Scale bars, 500 μm (C and E), 200 μm (A), and 50 μm (F and G).

These cells expressed a comprehensive set of markers that are considered to define hTSPCs: CD44, CD90, CD105, and CD146 (Fig. 1D) [12,29]. The cells were negative for hematopoietic markers such as CD34. That they were also negative for CD18 is consistent with a previous study [12], and further confirmed these tendon-derived cells were hTSPCs.

Osteogenic differentiation assays showed that most of the cells had mineralized calcium deposits, as confirmed by Von Kossa staining after three weeks of induction (Fig. 1E). The chondrogenic differentiation of hTSPCs was verified by positive safranin O staining after 4 weeks of mass culture and induction (Fig. 1G). The cells also had the capacity to undergo adipogenic differentiation. This was evident through the accumulation of lipid droplets after induction for three weeks (Fig. 1F).

3.2. Fabrication and morphological characterization of scaffold

The surface morphology of both aligned and random scaffolds was examined under SEM (Fig. 2 A and B). The diameters of the fibers of both fibrous scaffolds were comparable (430 ± 170 vs. 450 ± 110 nm). Most of the fibers in the aligned scaffolds formed angles from 0° to 10° with respect to the vertical axis, while the randomly-oriented scaffolds showed equal distributions at all angles (Fig. 2 C and D). Hence, the aligned fibers can be considered to be parallel.

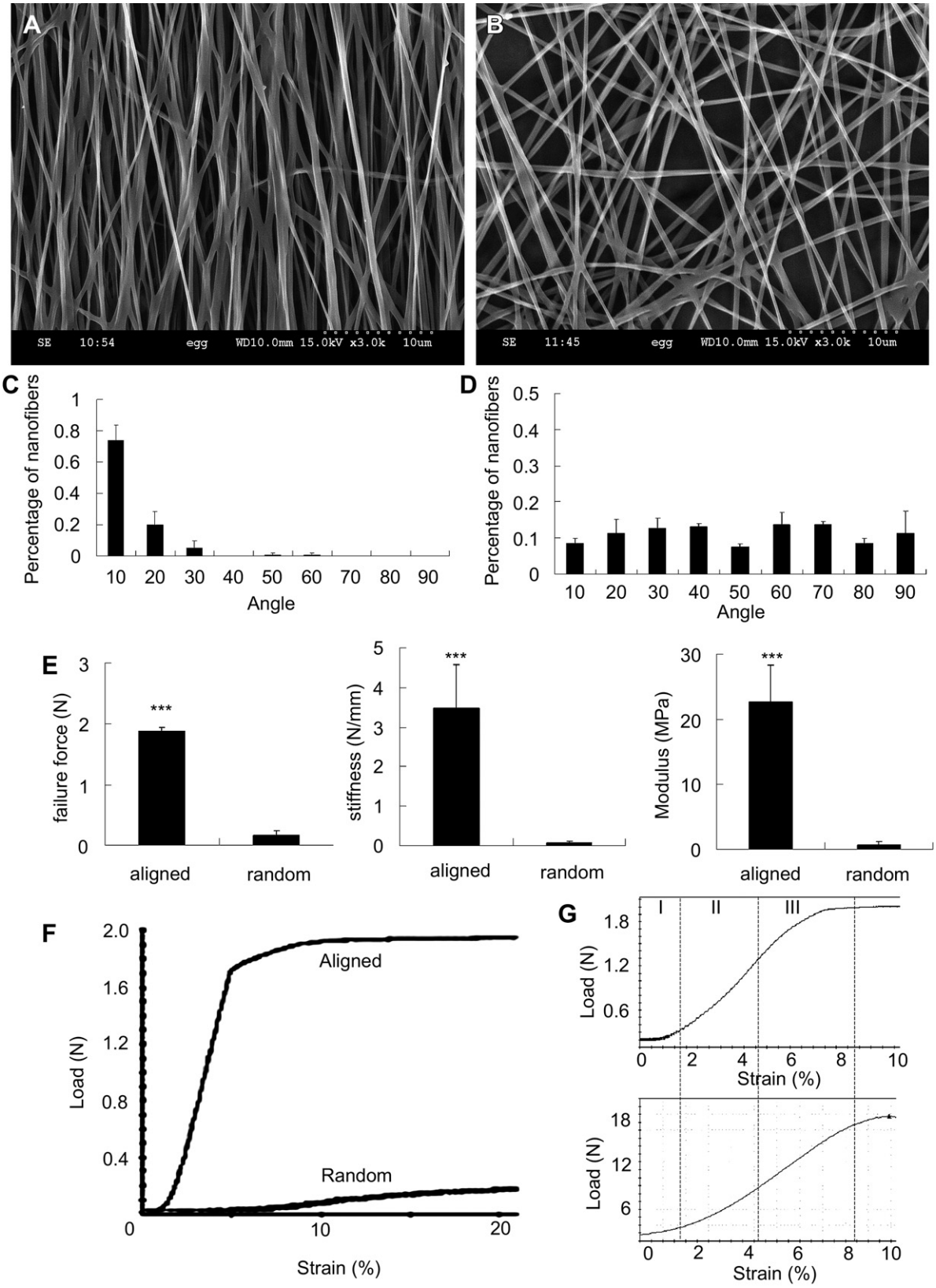

Fig. 2. (A) and (B) SEM micrographs (3000×) of electrospun PLLA with aligned (A) and randomly-oriented (B) fibrous scaffold surface morphology. Scale bars, 10 μm (C) and (D) Histograms representing angular distributions of aligned and randomly-oriented nanofibers, respectively. (E) Mechanical properties of electrospun scaffolds. Failure force, stiffness, and Young's modulus of aligned scaffold were significantly higher than randomly-oriented scaffold ($n = 5$, $p < 0.001$). (F) Load–strain curves of aligned and randomly-oriented fibrous scaffolds. (G) Load–strain curves of aligned scaffold (upper) and rabbit native tendon (lower), which are composed of "toe" (I), "linear" (II), and "failure"(III) regions.

3.3. Mechanical properties of the scaffold

As tendons are subjected to dynamic mechanical forces *in vivo*, the appropriate mechanical properties are required for ideal scaffolds. The mechanical properties of the aligned scaffold gave much higher values than the random scaffold. The stiffness of the aligned scaffold was 46 times that of the random group (3.48 ± 1.09 vs. 0.07 ± 0.04 N/mm; $p < 0.001$), the failure force of the aligned scaffold was 10-fold that of the random group (1.88 ± 0.05 vs. 0.17 ± 0.06 N; $p < 0.001$), and the modulus of the aligned scaffold was 36 times than that of the random group (22.76 ± 5.63 vs. 0.63 ± 0.56 MPa; $p < 0.001$) (Fig. 2E).

Moreover, the force–strain curve of the aligned scaffold was similar to native tendon, which is composed of aligned collagen fibers (Fig. 2G). The typical load–deformation and load–strain curves of the aligned scaffold demonstrated the typical behavior of tendon, which comprised a toe region (tendon not under stress, strain 1.5%), a linear region (recruitment of collagen fibers under stress, strain 1.5–4%), and a microfailure region (instability in the curve just before failure, >4%) [30] (Fig. 2G). But the force–strain curves of the random scaffold did not have such typical regions (Fig. 2F).

3.4. In vivo cytotoxity, cell orientation, and matrix arrangement

First, we implanted just the fibrous scaffolds in mouse skeletal muscle to see whether the matrix topography influences native tissue remodeling. Although cells were most concentrated at the scaffold periphery on day 7, cells and matrix completely covered the scaffold and penetrated it throughout by 6 weeks (Fig. 3). Hematoxylin and eosin-stained longitudinal sections of the aligned samples demonstrated a linear distribution of cells, which exhibited spindle-shaped morphology along the direction of the nanofibers (Fig. 3 A and C). Masson trichrome staining showed that more oriented collagen bundles formed in aligned than in randomly-oriented scaffolds (Fig. 3 G and H). In contrast, a random distribution of cells and matrix was observed in the histological images from randomly-oriented samples (Fig. 3 B, D, F and H). These results revealed that the aligned scaffold influenced and guided native cell organization *in vivo,* as well as the orientation of collagen fibers.

3.5. Cellular and nuclear morphology and proliferation

Morphological change was the first direct response to different scaffolds. The SEM micrographs indicated that hTSPCs were well attached to both scaffolds and showed that the cells on the randomly-oriented scaffolds exhibited a stellate-patterned phenotype (Fig. 4 B and F). In contrast, cells showed the classic fibroblastic phenotype on the aligned nanofibers; cells became gradually more elongated, expressing a spindle-shaped morphology extending parallel to the substrate nanofibers (Fig. 4 A and E). These data provide evidence that hTSPCs sense topographic differences. Some cells were seen under thin fibers, suggesting that cells crawled or spread inside the scaffold. Meanwhile, the SEM images of hTSPCs both on aligned and random scaffolds showed that filament-like extensions from the cell body attached to the nanofibers (Fig. 4 C and D); these were suspected to be focal adhesions. However, most of the filament-like structures on aligned scaffolds appeared at the extremities of the elongated cells (Fig. 4C, arrow), whereas these structures were seen on any parts of the cells on randomly-oriented scaffolds, which reveals that nanofibers influence the cell–matrix interaction. Under fluorescence microscopy, alignment of the cell nuclei was also apparent in propidium iodide staining, as the ovoid nuclei became more uniformly oriented in the direction of the nanofibers (Fig. 4E). But the cells cultured on the randomly-oriented scaffolds showed distinct morphology and random orientations (Fig. 4F), further confirming the effect of matrix guidance on cell morphology and growth. Comparing cell density measured at days 1, 3, 7, 11 and 14 on the electrospun aligned to randomly-oriented scaffolds so as to examine hTSPC attachment and proliferation, there was no statistical difference (Fig. 4G).

3.6. Cell differentiation induced by scaffold

We found that the aligned scaffold promoted teno-lineage differentiation more than the randomly-oriented scaffold (Fig. 5). The transcription factor genes scleraxis and eya2, and the matrix gene collagen XIV, were elevated significantly at day 3, and their expression was much higher than in the randomly-oriented scaffold (Fig. 5A). However, the differences in the expression of these genes between the two groups diminished at day 7, perhaps because the effect of alignment initiated cell differentiation to the teno-lineage. Meanwhile, collagen I and III, which are also bone matrix genes, were relatively higher in the randomly-oriented group at day 3, whereas elastin was expressed relatively more in the aligned group (Fig. 5A). The lack of significant differences in the expression of type I and III collagen, even on day 7, was attributable in part to the fact that they are also bone matrix components. In addition, osteocalcin and

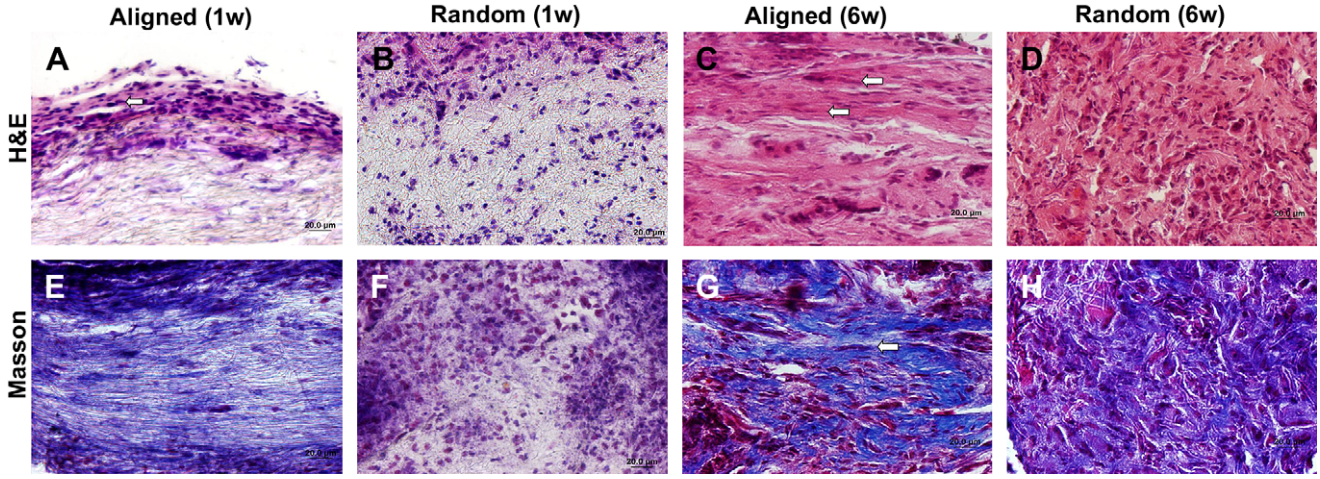

Fig. 3. Histological appearance of cell orientation and matrix arrangement induced by electrospun nanofibers *in vivo* for 1 and 6 weeks. Typical hematoxylin and eosin staining (A–D) shows histological appearance of fibrous scaffold-induced tissue formation. Masson trichrome staining (E–H) shows the bands of collagen fibers formed in the fibrous scaffold. Scale bars, 20 μm (A–H). Arrows show the cell alignment and the cells present against the fibrous scaffold.

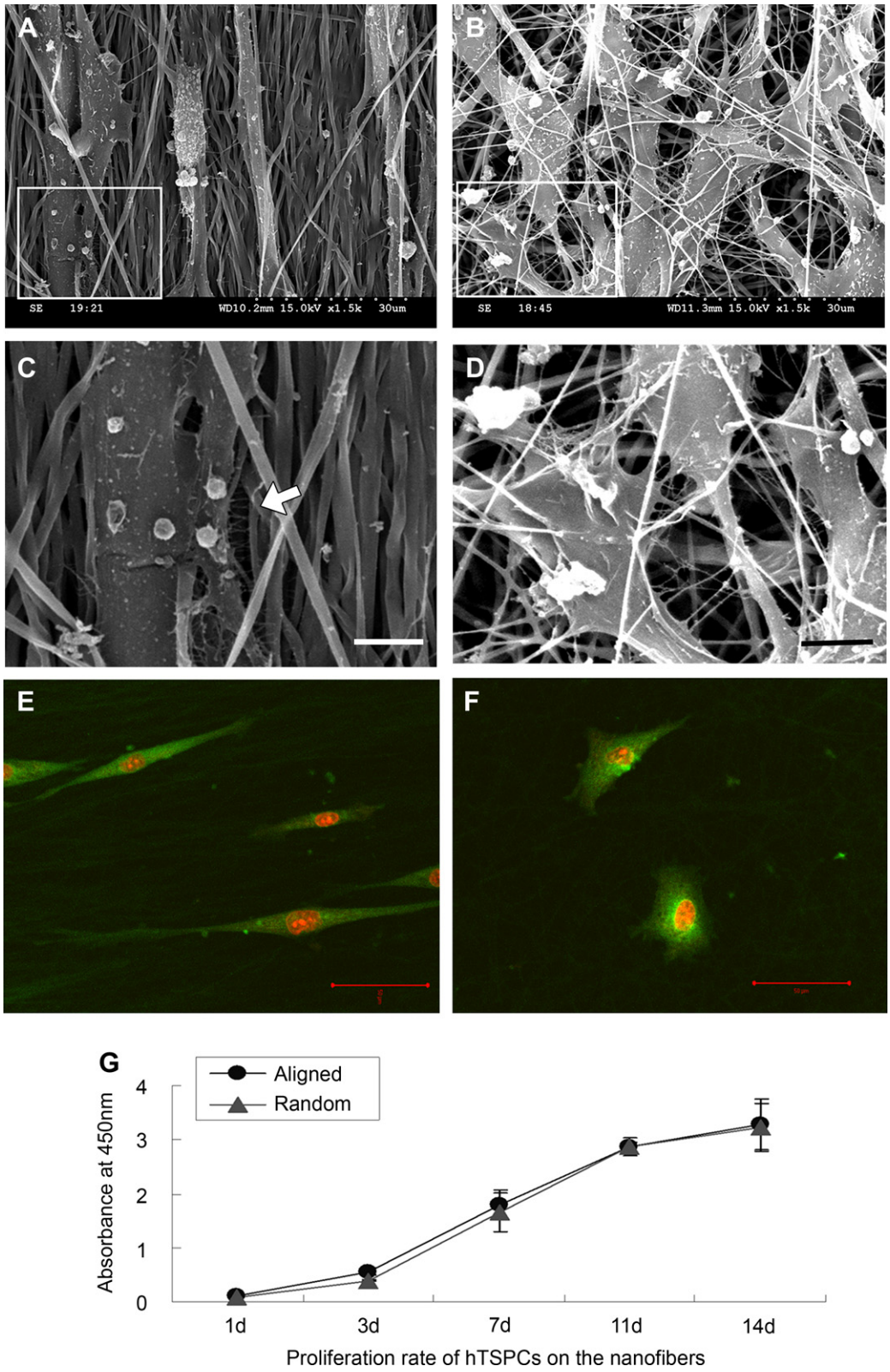

Fig. 4. Morphological changes of hTSPCs growing on the scaffolds. (A) and (B) show hTSPCs cultured on the aligned and randomly-oriented scaffold respectively. (C) and (D) High magnification of boxed areas in (A) and (B) show the cell–matrix adhesion between hTSPCs and PLLA nanofibers. Arrow in (C) indicates filament-like structure on aligned scaffold. (E) Confocal micrograph of CFDA-stained elongated hTSPCs on the aligned scaffold. (F) Confocal micrograph showing the morphological change of CFDA-stained hTSPCs on the randomly-oriented scaffold. (G) Cell proliferation on the aligned and randomly-oriented scaffolds. Scale bars, 30 μm (A and B), 5 μm (C and D) and 50 μm (E and F).

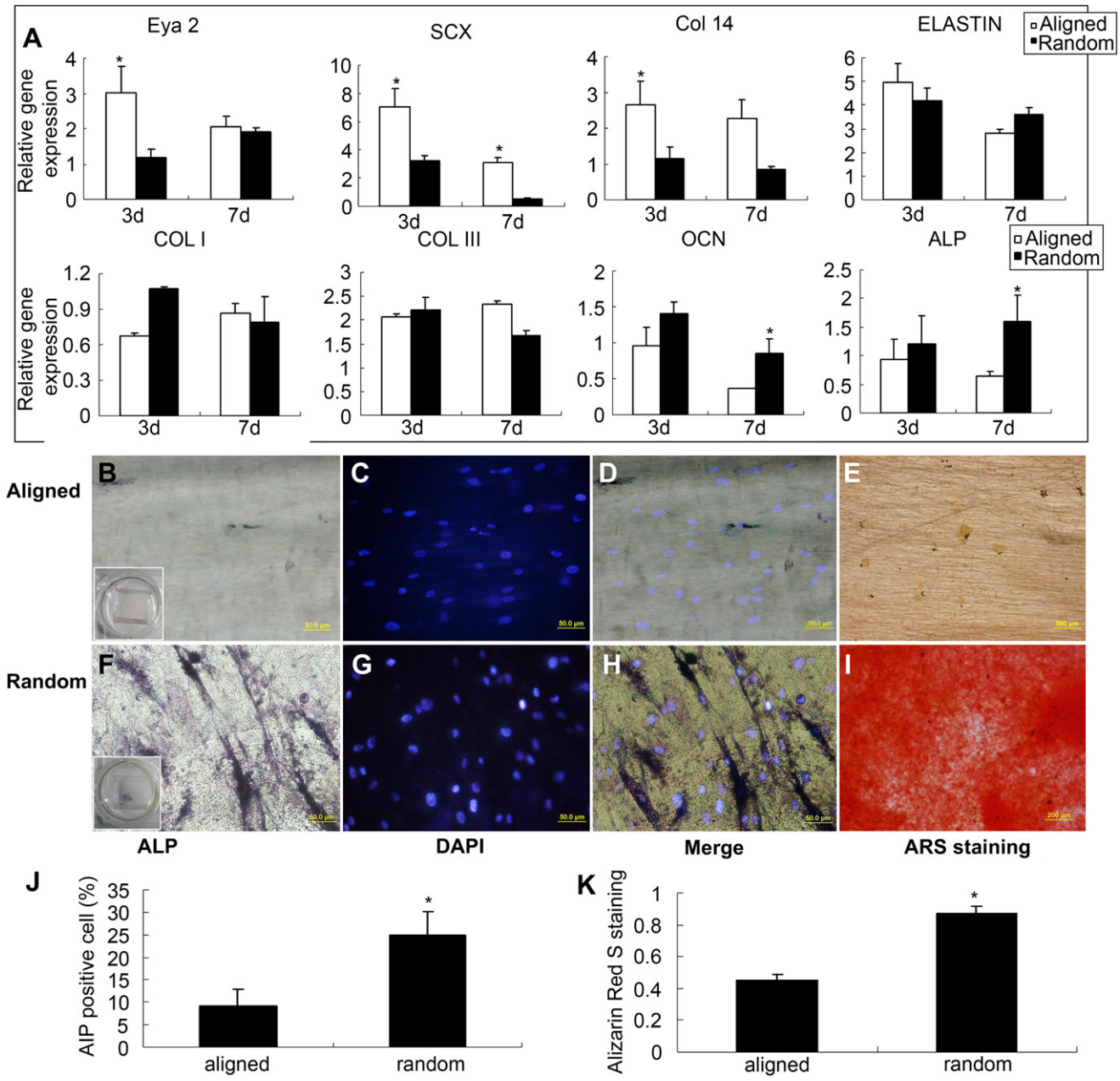

Fig. 5. (A) Expression of tendon-specific and related matrix genes by hTSPCs cultured on the aligned and randomly-oriented scaffolds for 3 and 7 days. Levels, quantified using real-time RT-PCR, are normalized to the housekeeping gene, β-actin. (B) and (F) ALP staining of hTSPCs cultured on the aligned and randomly-oriented scaffolds in normal induction media for 2 weeks, respectively. Insets show macroscopic appearance. (C) and (G) show hTSPC nuclei stained with DAPI. (D) Merged images of (B) and (C). (H) Merged images of (F) and (G). (E) and (I) Alizarin red S staining of hTSPCs cultured on the aligned and randomly-oriented scaffolds in normal induction media for 2 weeks, respectively. (J) Percentages of ALP-positive cells on aligned and random scaffolds. Data are mean ± SD, $n = 5$, $p < 0.05$. (K) Quantification results of alizarin red S staining by absorbance at 405 nm. Scale bars, 50 μm (B–D and F–H), 200 μm (E), 500 μm (I).

ALP expression were significantly upregulated in the randomly-oriented group compared with the aligned group, which implies that random nanofibers stimulate stem cell differentiation to the osteo-lineage. Accordingly, ALP staining confirmed the expression of ALP, with a higher level detected in the randomly-oriented group (Fig. 5 F–H and J). This was accompanied by an increase in mineralization, as shown by alizarin red S staining (Fig. 5 I and K). In the aligned group, both staining tests were apparently negative (Fig. 5 B–E). These results indicate that cell orientation induced by nanotopography plays an important role in cell differentiation.

As recently reported by Hoffman et al. [31], tenogenesis and osteogenesis share a common pathway. BMP2, which is a strongly osteogenic growth factor, can also induce tendon-lineage differentiation under special conditions. To evaluate the effects of aligned nanofibers on inducing tenogenesis, we combined physical and chemical cues. We examined the expression of osteogenic transcription factor as well as tendon-specific genes in the osteogenic induction culture. The expression of the osteogenic transcription factor runt-related transcription factor (Runx 2) and ALP was significantly enhanced in hTSPCs cultured on the randomly-oriented scaffold at day 3. Most strikingly, these osteogenesis-related genes were expressed at markedly low levels in hTSPCs growing on the aligned scaffold, even in osteogenic medium (Fig. 6 A). Real-time PCR also showed that hTSPCs on the aligned scaffolds

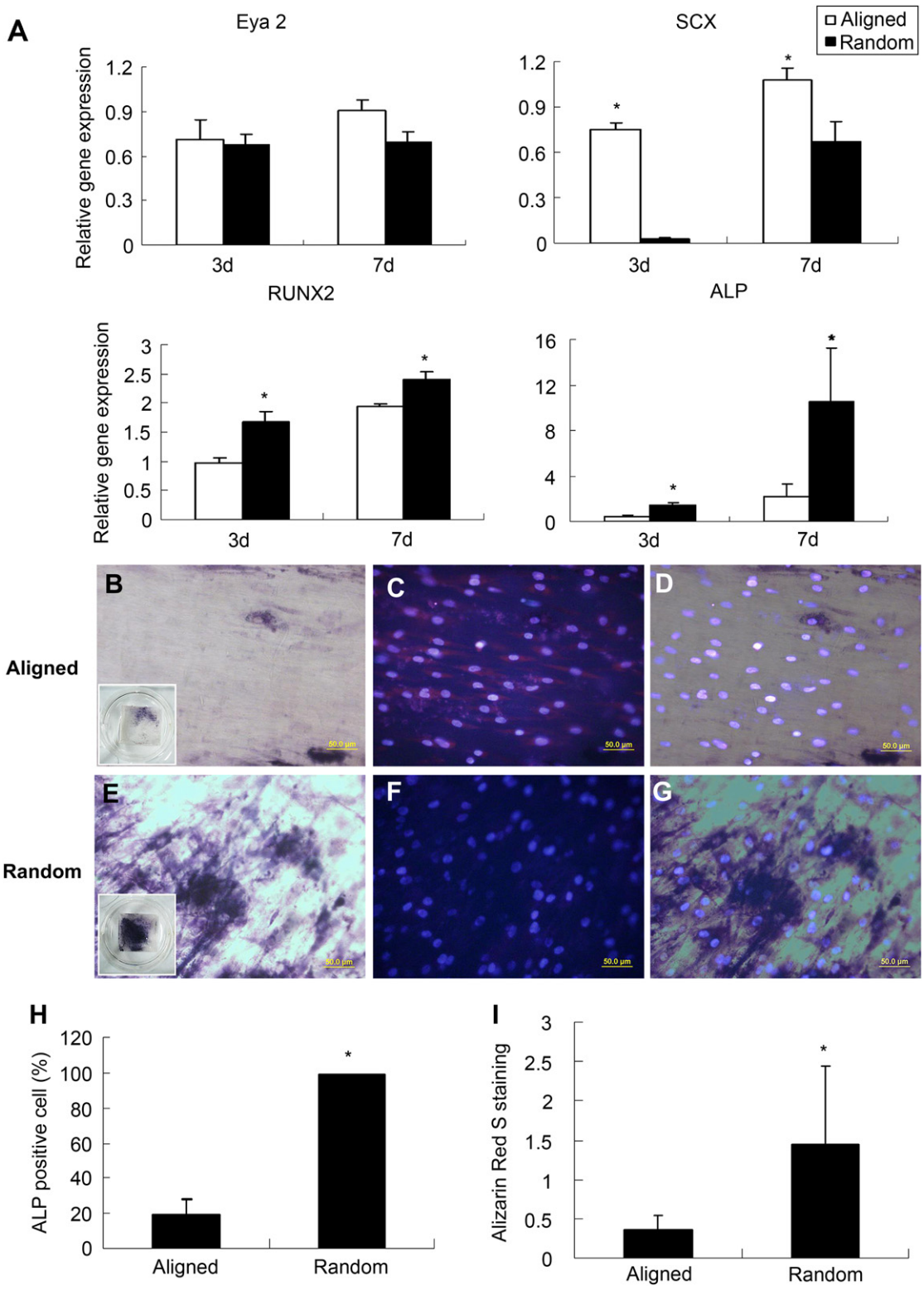

Fig. 6. (A) Expression of tendon-specific and osteogenic genes by hTSPCs cultured on the aligned and randomly-oriented scaffolds in osteogenic induction medium for 3 and 7 days. Levels, quantified using real-time RT-PCR, are normalized to the housekeeping gene, β-actin. (B) and (E) ALP staining of hTSPCs cultured on the aligned and randomly-oriented scaffolds in osteogenic induction media for 2 weeks, respectively. Insets show macroscopic appearance. (C) and (F) show hTSPC nuclei stained with DAPI. (D) Merged images of (B) and (C). (G) Merged images of (E) and (F). (H) Percentages of ALP-positive cells on aligned and random scaffolds. Data are mean ± SD, $n = 5$, $p < 0.05$. (I) Quantification results of alizarin red S staining by absorbance at 405 nm. Scale bars, 50 μm (B–G).

expressed greater amounts of the tenogenic transcriptional factors scleraxis and eya2 than on randomly-oriented scaffolds following the addition of osteogenic factors (Fig. 6A). Expression of the matrix genes collagen III and elastin showed no significant differences between the groups (data not shown). ALP and alizarin red S staining were taken to confirm the real-time results after hTSPCs were cultured in osteogenic induction medium for 2 weeks (Fig. 6 B and E). DAPI-stained nuclei indicate cell location in the fibrous scaffold (Fig. 6 C and F). The number of ALP-positive cells was significantly smaller on the aligned than on the random scaffold (Fig. 6 D, G and H). Quantification of alizarin red S staining gave consistent results that lineage commitment induced by the aligned matrix resisted osteogenic differentiation (Fig. 6I). Although soluble factors are commonly regarded as being the effectors that control cell fate, matrix topography provides equally important instructions for controlling gene expression and the fate of hTSPCs. These results suggest that attachment to the aligned nanofibers promotes teno-lineage differentiation of hTSPCs and maintains this trend even in osteogenic induction medium.

It is known that cell–matrix interaction, which is mediated by integrin, plays an important role in regulating cell functions such as migration, proliferation, and differentiation [32]. Interestingly, the expression of all integrin subunits was upregulated after culture on the aligned scaffold and to a higher degree than the random scaffold (Fig. 7). Moreover, an intriguing result showed that non-muscle myosin II B also increased significantly in hTSPCs on the aligned scaffold. But both the integrin subunits and myosin II B exhibited levels that were almost unchanged after hTSPCs were cultured on the random scaffold for 3 days. By day 7, there were no significant differences in integrin and myosin II B expression between the two groups. This was consistent with the results for tendon-specific gene expression. Nonmuscle myosin IIB is likely to be involved in exerting force through the adhesion complex in mechanisms of sensing topographic cues. These results indicated that cell orientation, and even differentiation, induced by aligned nanofibers is related to the integrin-mediated signaling cascades that control cytoskeletal organization, gene regulation, and diverse cellular functions. Further research is required to clarify the mechanisms underlying matrix topography induction.

3.7. *In vivo study*

Before seeding on the scaffold, the TSPCs were stained with DiI (Fig. 8 A). After 1 week *in vivo*, the collagen content was higher in the aligned constructs than in the random constructs (Fig. 8B). We found that on aligned scaffolds, a great number of cells exhibited spindle-shaped morphology and organized collagen deposition with respect to the underlying surface topography at one week (Fig. 8C). Consistent with the *in vitro* results, the cells on random scaffolds showed round shapes and non-preferential arrangement (Fig. 8D). Masson trichrome staining showed the tissue matrix of the aligned constructs was denser, while the random scaffolds were filled with loose, disarranged soft tissues (Fig. 8 E and F). Detection of DiI-tracked hTSPCs showed that implanted hTSPCs participated in the ectopic new tissue regeneration in both groups (Fig. 8 G and H). This reflected that the aligned scaffold induced spindle-shaped cells and tendon-like tissue *in vivo* and enhanced extracellular matrix production and arrangement.

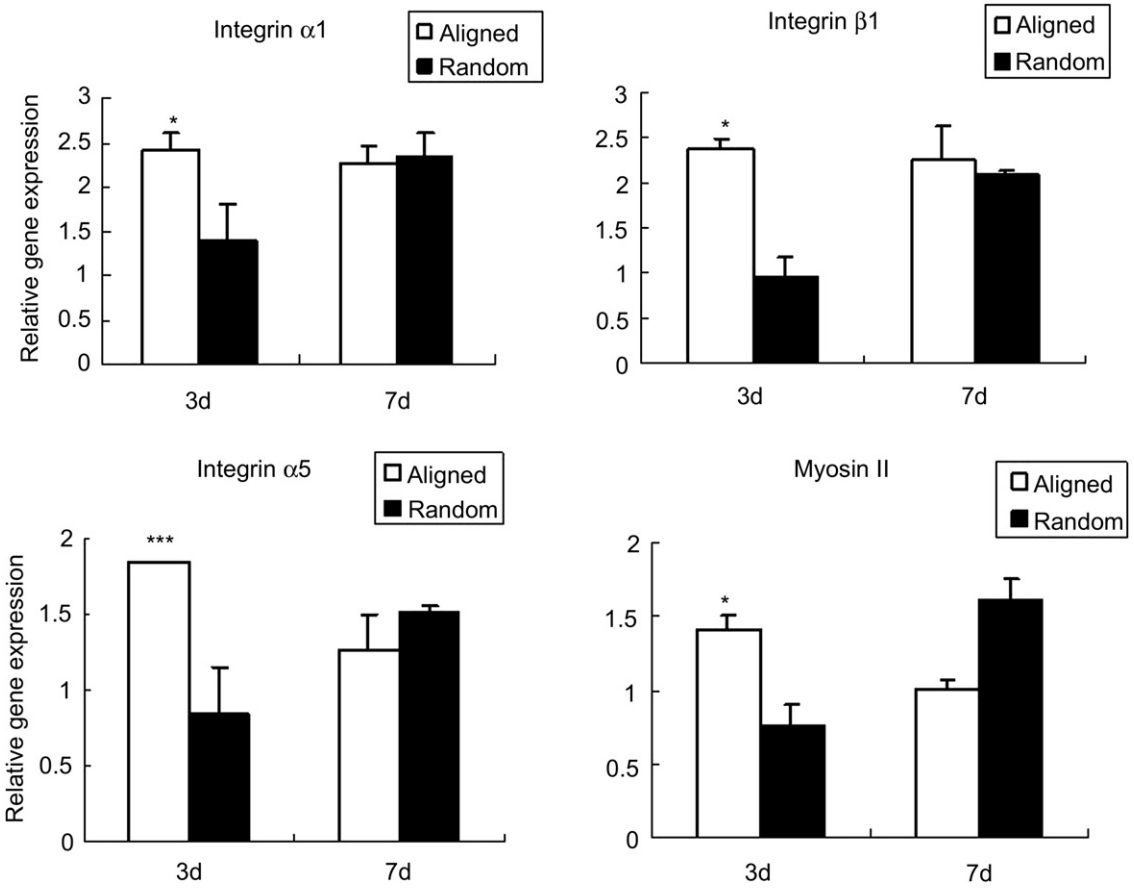

Fig. 7. Expression of integrin subunits by hTSPCs cultured on the aligned and randomly-oriented scaffolds for 3 and 7 days. Levels, quantified using real-time RT-PCR, are normalized to the housekeeping gene, β-actin.

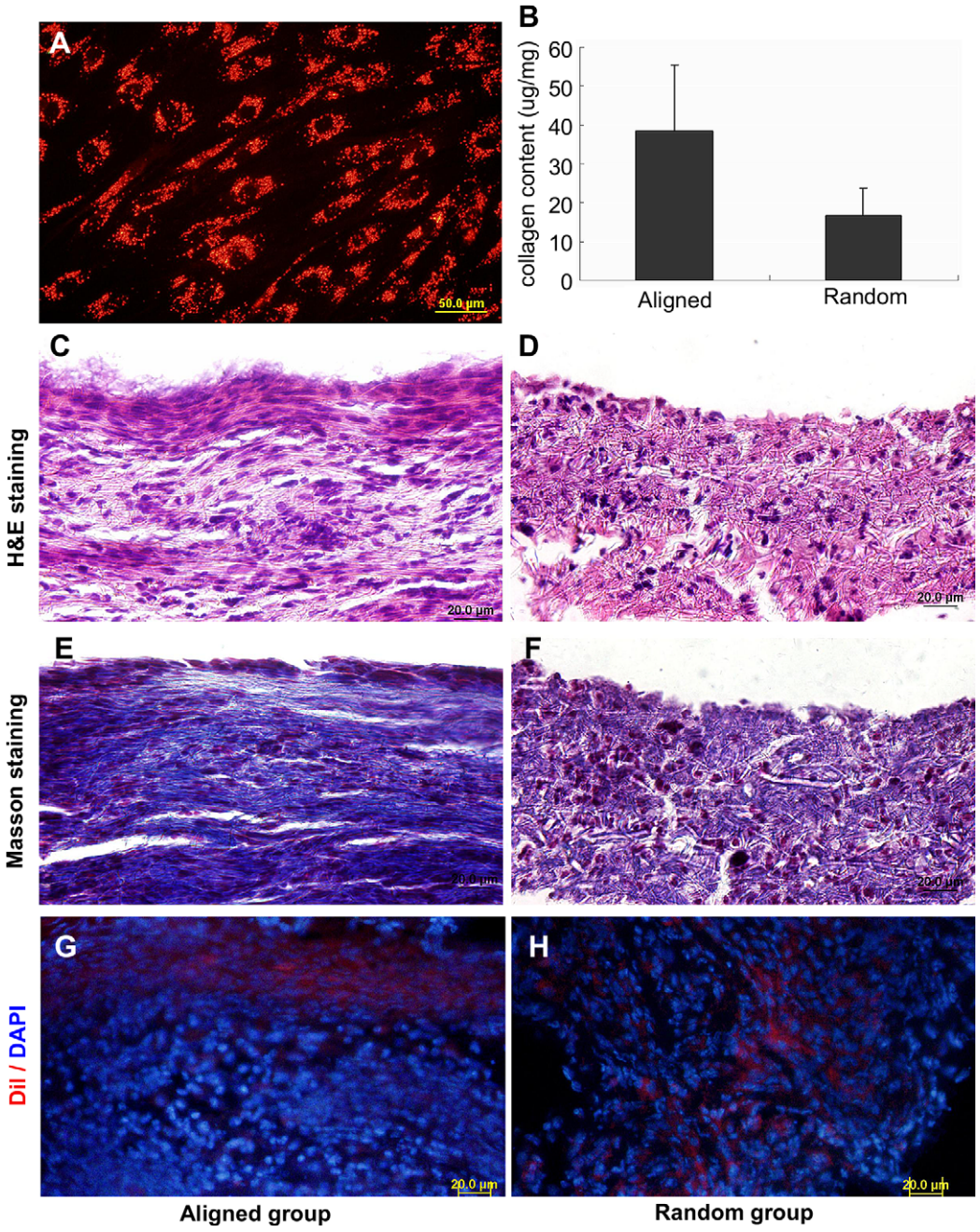

Fig. 8. Histology of hTSPCs cultured on scaffolds implanted subcutaneously in nude mice 1 week after surgery. (A) DiI-stained hTSPCs before seeding on the scaffold. (B) Collagen content assay results showed aligned constructs had higher collagen content. (C) and (D) Typical hematoxylin and eosin staining of aligned and randomly-oriented constructs, respectively. (E) and (F) Masson trichrome staining of aligned and randomly-oriented constructs, respectively. (G) Fluorescence of the aligned construct section showed the hTSPCs survived and formed tendon-like tissue at 1 week. (H) Fluorescence of the random construct section showed the hTSPCs survived. Red represents DiI-stained hTSPCs, blue shows DAPI-stained nuclei. Scale bars, 20 μm (C–H).

4. Discussion

The present study focused on demonstrating that aligned nanofibers induce teno-lineage differentiation of human tendon stem cells as evidenced by a significant up-regulation of tendon-specific markers. Also, this aligned scaffold induced spindle-shaped cells and tendon-like tissue *in vivo*. More importantly, this matrix-specified lineage resisted the power of an osteogenic induction medium. Furthermore, the aligned scaffold influenced the differentiation of hTSPCs through an integrin-mediated mechano-transduction pathway. Collectively, these findings illustrate the relationship between the alignment of the scaffold and the differentiation of tendon stem cells as well as suggesting the potential of aligned nanofibers to induce and support tendon regeneration.

Adult tendon stem/progenitor cells regenerate tendon-like tissue both *in vitro* and *in vivo* and provide an ideal cell source for treating damaged tendon tissue [33]. In this study, we isolated, identified, and used fetal hTSPCs to investigate cell–matrix interactions and tendon regeneration. Only fetal tendons can regenerate, and they lose this ability during development [34,35]. This capacity for regeneration is intrinsic to the fetal tendon itself, because transplanting fetal tendons into the adult environment has

no effect on their ability to heal in a regenerative fashion [34]. Thus, fetal tendon cells play a crucial role in regeneration. We found that fetal hTSPCs possess a high capacity for colony formation and the phenotype and multipotency are similar to those of bone marrow stromal cells and adult hTSPCs [12]. Therefore, fetal hTSPCs provide an attractive model for studies of cell–matrix interactions and tendon regeneration.

As tenocytes are known to be surrounded mainly by nano-topography in their natural extracellular environment, we designed an aligned fibrous membrane as a scaffold to direct the specification of hTSPC lineage. In this study, the nanofibers produced by electrospinning not only mimicked the dimensions of the constituent components in tendon, but were also organized in a parallel manner creating a defined orientation. We found that the aligned scaffold promoted teno-lineage differentiation of hTSPCs based on cell morphology, cell alignment, and tendon-specific gene expression. Although there are no tendon-specific genes, some genes, such as scleraxis, six1, and eya2, are associated with teno-lineage differentiation [31]. Moreover, the functional gene expression of tenocytes, such as matrix gene collagen I, III, XIV, and elastin [36], were used to evaluate the tendon-lineage differentiation [31]. The expression levels of markers of tendon-lineage were higher while the levels of osteogenic markers were lower in the aligned hTSPCs than those on the randomly-oriented scaffold. Morphological changes, cytoskeletal rearrangements, and nuclear elongation have also been reported in other cell types in response to aligned nanotopography [24,37,38]. The aligned nanofibers are suitable for ligament cell proliferation and orientation under a mechanical stimulus [39], and scaffolds with an aligned nanotopography are effective in enhancing axon extrusion from neuronal stem cells [24,40]. However, these studies mainly illustrate the effects of aligned nanotopography on cell morphology.

Moreover, it was surprising to find that the alignment of nanofibers significantly hindered the osteo-lineage differentiation of hTSPCs when cultured under osteogenic conditions. This intriguing finding reflects that an aligned nanotopography exerts an "instructive" function as effectively as chemical cues. In one study, a random nanopattern was used to drive mesenchymal stem cells to transform into osteoblast-like cells [20]. Since stem cells for tendon repair may cause ectopic bone formation [10], our findings suggest that the use of aligned nanofibers not only promotes tendon stem cell differentiation to the teno-lineage but also supports cells to resist osteogenic factors *in vitro*.

The aligned PLLA fibrous membranes were fabricated by electrospinning using a simple rotating collector. This relatively economic and controllable technique is widely used [41]. The advantage of this nanofiber scaffold over other patterned scaffolds produced by lithography, is that it is easily tailored and is suitable for *in vivo* studies. Tenocyte-like cells and the orientation of the collagen matrix guided by nanofibers *in vivo* may help repaired tendon to achieve its native functions. The functional and biocompatible properties of this biomaterial scaffold could lead to the development of engineered implant materials that can organize and align cell populations to facilitate desirable cell–cell interactions and promote tissue formation.

The integrins mediate cell–matrix interactions and provide a bi-direction transducer of mechanochemical information between extracellular and intracellular compartments [42]. Downstream signaling cascades via integrins control cytoskeletal organization, gene regulation, and diverse cellular processes and functions. In this study, expression of all of the integrin subunits examined, $\alpha 1$, $\alpha 5$, and $\beta 1$, significantly increased in cells growing on the aligned scaffold compared with those in the randomly-oriented scaffold, both with and without osteogenic induction medium. Previous work showed that under conditions of strain, expression of the $\alpha 5$ and $\beta 1$ integrin subunits increases remarkably, and is accompanied by the alignment of cells and collagen parallel to an applied strain [43]. Non-muscle myosin II, the cytoskeletal motor, is likely involved in matrix-elasticity sensing, and focal adhesion of mesenchymal stem cells increases with myosin II-based contractility [19]. And a recent study of cell–matrix interactions reveals that non-myosin II B is required in integrin-mediated transport of collagen fibers and subsequent contraction [44]. Results from our study also showed high-level expression of myosin II B in the oriented cells, reflecting strong actin–myosin contractions. In response, the cell may drive cytoskeletal reorganization to conform to the anisotropic mechanical environment and result in clear orientation as well as morphological change and elongation. This process is likely independent of soluble factors, and may be the reason for sustaining teno-lineage in an osteogenic medium. The lineage-specific differentiation of hTSPCs was accompanied by dramatic changes in cell morphology and orientation, likely in part due to changes in expression of integrins and myosin. Here, investigations into the mechanism of topography-induced hTSPC commitment highlight the importance of cell–matrix interactions and the mechanochemical signals they transduce in ultimately determining stem cell fate.

5. Conclusion

This study demonstrates that aligned electrospun nanofibers provide an instructive microenvironment for hTSPCs to differentiate into the teno-lineage. Moreover, we found that this topography-driven commitment is related to integrin- and myosin-mediated mechanotransduction. This study contributes to understanding the biological activity of hTSPCs on nanofibrous scaffolds, and may lead to the development of desirable engineered tendons composed of optimal stem cells and smart scaffolds which can organize and align cell populations to facilitate differentiation to the tendon-lineage.

Acknowledgement

The authors thank Chen Han-Ming for the SEM observations. This work was supported by the National Natural Science Foundation of China (30600301, 30600670, U0672001), Zhejiang Province grants (R206016, 2006C 14024, 2006C 13084), and the Foundation of Zhejiang Provincial Key Medical Discipline (Medical Tissue Engineering).

Appendix

Figures with essential color discrimination. Figs. 1, 3–6 and 7 in this article are difficult to interpret in black and white. The full color images can be found in the on-line version, at doi:10.1016/j.biomaterials.2009.11.083.

References

[1] Woo SL, Debski RE, Zeminski J, Abramowitch SD, Saw SS, Fenwick JA. Injury and repair of ligaments and tendons. Annu Rev Biomed Eng 2000;2:83–118.
[2] Coons DA, Alan Barber F. Tendon graft substitutes-rotator cuff patches. Sports Med Arthrosc 2006;14:185–90.
[3] Vunjak-Novakovic G, Altman G, Horan R, Kaplan DL. Tissue engineering of ligaments. Annu Rev Biomed Eng 2004;6:131–56.
[4] Goh JC, Ouyang HW, Teoh SH, Chan CK, Lee EH. Tissue-engineering approach to the repair and regeneration of tendons and ligaments. Tissue Eng 2003;9(Suppl. 1):S31–44.
[5] Olson EJ, Kang JD, Fu FH, Georgescu HI, Mason GC, Evans CH. The biochemical and histological effects of artificial ligament wear particles: in vitro and in vivo studies. Am J Sports Med 1988;16:558–70.
[6] Ouyang HW, Cao T, Zou XH, Heng BC, Wang LL, Song XH, et al. Mesenchymal stem cell sheets revitalize nonviable dense grafts: implications for repair of large-bone and tendon defects. Transplantation 2006;82:170–4.

[7] Ge Z, Goh JC, Lee EH. The effects of bone marrow-derived mesenchymal stem cells and fascia wrap application to anterior cruciate ligament tissue engineering. Cell Transplant 2005;14:763–73.
[8] Chong AK, Ang AD, Goh JC, Hui JH, Lim AY, Lee EH, et al. Bone marrow-derived mesenchymal stem cells influence early tendon-healing in a rabbit achilles tendon model. J Bone Jt Surg Am 2007;89:74–81.
[9] Liu W, Chen B, Deng D, Xu F, Cui L, Cao Y. Repair of tendon defect with dermal fibroblast engineered tendon in a porcine model. Tissue Eng 2006;12:775–88.
[10] Harris MT, Butler DL, Boivin GP, Florer JB, Schantz EJ, Wenstrup RJ. Mesenchymal stem cells used for rabbit tendon repair can form ectopic bone and express alkaline phosphatase activity in constructs. J Orthop Res 2004;22:998–1003.
[11] Ge Z, Goh JC, Lee EH. Selection of cell source for ligament tissue engineering. Cell Transplant 2005;14:573–83.
[12] Bi Y, Ehirchiou D, Kilts TM, Inkson CA, Embree MC, Sonoyama W, et al. Identification of tendon stem/progenitor cells and the role of the extracellular matrix in their niche. Nat Med 2007;13:1219–27.
[13] Dalby MJ, McCloy D, Robertson M, Agheli H, Sutherland D, Affrossman S, et al. Osteoprogenitor response to semi-ordered and random nanotopographies. Biomaterials 2006;27:2980–7.
[14] Recknor JB, Recknor JC, Sakaguchi DS, Mallapragada SK. Oriented astroglial cell growth on micropatterned polystyrene substrates. Biomaterials 2004;25:2753–67.
[15] Recknor JB, Sakaguchi DS, Mallapragada SK. Directed growth and selective differentiation of neural progenitor cells on micropatterned polymer substrates. Biomaterials 2006;27:4098–108.
[16] Guilak F, Cohen DM, Estes BT, Gimble JM, Liedtke W, Chen CS. Control of stem cell fate by physical interactions with the extracellular matrix. Cell Stem Cell 2009;5:17–26.
[17] Keselowsky BG, Wang L, Schwartz Z, Garcia AJ, Boyan BD. Integrin alpha(5) controls osteoblastic proliferation and differentiation responses to titanium substrates presenting different roughness characteristics in a roughness independent manner. J Biomed Mater Res A 2007;80:700–10.
[18] Silva GA, Czeisler C, Niece KL, Beniash E, Harrington DA, Kessler JA, et al. Selective differentiation of neural progenitor cells by high-epitope density nanofibers. Science 2004;303:1352–5.
[19] Engler AJ, Sen S, Sweeney HL, Discher DE. Matrix elasticity directs stem cell lineage specification. Cell 2006;126:677–89.
[20] Dalby MJ, Gadegaard N, Tare R, Andar A, Riehle MO, Herzyk P, et al. The control of human mesenchymal cell differentiation using nanoscale symmetry and disorder. Nat Mater 2007;6:997–1003.
[21] Kannus P. Structure of the tendon connective tissue. Scand J Med Sci Sports 2000;10:312–20.
[22] Hoffmann A, Gross G. Tendon and ligament engineering in the adult organism: mesenchymal stem cells and gene-therapeutic approaches. Int Orthop 2007;31:791–7.
[23] Boudreau NJ, Jones PL. Extracellular matrix and integrin signalling: the shape of things to come. Biochem J 1999;339(Pt 3):481–8.
[24] Yang F, Murugan R, Wang S, Ramakrishna S. Electrospinning of nano/micro scale poly(L-lactic acid) aligned fibers and their potential in neural tissue engineering. Biomaterials 2005;26:2603–10.
[25] Pittenger MF, Mackay AM, Beck SC, Jaiswal RK, Douglas R, Mosca JD, et al. Multilineage potential of adult human mesenchymal stem cells. Science 1999;284:143–7.
[26] Bi Y, Stuelten CH, Kilts T, Wadhwa S, Iozzo RV, Robey PG, et al. Extracellular matrix proteoglycans control the fate of bone marrow stromal cells. J Biol Chem 2005;280:30481–9.
[27] Livak KJ, Schmittgen TD. Analysis of relative gene expression data using real-time quantitative PCR and the 2(-Delta Delta C(T)) Method. Methods 2001;25:402–8.
[28] Ivey KN, Muth A, Arnold J, King FW, Yeh RF, Fish JE, et al. MicroRNA regulation of cell lineages in mouse and human embryonic stem cells. Cell Stem Cell 2008;2:219–29.
[29] de Mos M, Koevoet WJ, Jahr H, Verstegen MM, Heijboer MP, Kops N, et al. Intrinsic differentiation potential of adolescent human tendon tissue: an in-vitro cell differentiation study. BMC Musculoskelet Disord 2007;8:16.
[30] Wang JH. Mechanobiology of tendon. J Biomech 2006;39:1563–82.
[31] Hoffmann A, Pelled G, Turgeman G, Eberle P, Zilberman Y, Shinar H, et al. Neotendon formation induced by manipulation of the Smad8 signalling pathway in mesenchymal stem cells. J Clin Invest 2006;116:940–52.
[32] Schwartz MA, Ginsberg MH. Networks and crosstalk: integrin signalling spreads. Nat Cell Biol 2002;4:E65–8.
[33] Aslan H, Kimelman-Bleich N, Pelled G, Gazit D. Molecular targets for tendon neoformation. J Clin Invest 2008;118:439–44.
[34] Favata M, Beredjiklian PK, Zgonis MH, Beason DP, Crombleholme TM, Jawad AF, et al. Regenerative properties of fetal sheep tendon are not adversely affected by transplantation into an adult environment. J Orthop Res 2006;24:2124–32.
[35] Beredjiklian PK, Favata M, Cartmell JS, Flanagan CL, Crombleholme TM, Soslowsky LJ. Regenerative versus reparative healing in tendon: a study of biomechanical and histological properties in fetal sheep. Ann Biomed Eng 2003;31:1143–52.
[36] Schweitzer R, Chyung JH, Murtaugh LC, Brent AE, Rosen V, Olson EN, et al. Analysis of the tendon cell fate using scleraxis, a specific marker for tendons and ligaments. Development 2001;128:3855–66.
[37] Zhu B, Lu Q, Yin J, Hu J, Wang Z. Alignment of osteoblast-like cells and cell-produced collagen matrix induced by nanogrooves. Tissue Eng 2005;11:825–34.
[38] Lenhert S, Meier MB, Meyer U, Chi L, Wiesmann HP. Osteoblast alignment, elongation and migration on grooved polystyrene surfaces patterned by Langmuir–Blodgett lithography. Biomaterials 2005;26:563–70.
[39] Lee CH, Shin HJ, Cho IH, Kang YM, Kim IA, Park KD, et al. Nanofiber alignment and direction of mechanical strain affect the ECM production of human ACL fibroblast. Biomaterials 2005;26:1261–70.
[40] Yim EK, Pang SW, Leong KW. Synthetic nanostructures inducing differentiation of human mesenchymal stem cells into neuronal lineage. Exp Cell Res 2007;313:1820–9.
[41] Martins A, Araujo JV, Reis RL, Neves NM. Electrospun nanostructured scaffolds for tissue engineering applications. Nanomed 2007;2:929–42.
[42] Berrier AL, Yamada KM. Cell–matrix adhesion. J Cell Physiol 2007;213:565–73.
[43] Henshaw DR, Attia E, Bhargava M, Hannafin JA. Canine ACL fibroblast integrin expression and cell alignment in response to cyclic tensile strain in three-dimensional collagen gels. J Orthop Res 2006;24:481–90.
[44] Meshel AS, Wei Q, Adelstein RS, Sheetz MP. Basic mechanism of three-dimensional collagen fibre transport by fibroblasts. Nat Cell Biol 2005;7:157–64.